Nanometer-scale water droplet free from the constraint of reverse micelles at low temperatures

H. Murakami,[1,*] T. Sada,[1,2] M. Yamada,[1,2] and M. Harada[2]

[1]*Kansai Photon Science Institute, Japan Atomic Energy Agency, Kyoto 619-0215, Japan*

[2]*Faculty of Human Life and Environment, Nara Women's University, Nara 630-8506, Japan*

(Received 5 November 2012; revised manuscript received 2 July 2013; published 7 November 2013)

Temperature dependence of the configurational fluctuation of water confined in a reverse micellar solution has been studied by absorption spectroscopy of a probe molecule. We have found that the configurational fluctuation is liquidlike below the homogeneous nucleation temperature. This is proposed to be due to a large reduction in the confinement of water, and is explained in terms of water shedding from the reverse micelle. Further, the configurational fluctuation is frozen at ∼210 K. A reverse micellar solution is considered to be a promising candidate for studies of supercooled water.

DOI: 10.1103/PhysRevE.88.052304 PACS number(s): 82.70.−y, 61.25.Em, 64.70.−p, 78.40.−q

I. INTRODUCTION

Considerable attention has been focused on supercooled water for several decades, since it was discovered that the thermodynamic properties of water, such as the isobaric specific heat and thermal expansion, appear to diverge at 228 K [1]. Several hypotheses were proposed to explain a number of anomalous properties of water in a unified way [2,3]. However, the existence of thermodynamic singularity at 228 K has yet to be verified experimentally, and it is unclear which of the existing hypotheses leads to a valid model of water [2,3]. One difficulty with experimental investigations of supercooled water is the presence of homogeneous nucleation to an ice crystal at ∼235 K and atmospheric pressure. On the other hand, it is commonly believed that the glass transition of water occurs at ∼136 K. However, Angel and co-workers suggested that the transition occurs above ∼160 K [4], and the controversy on the transition point has continued [5]. Accordingly, it is difficult to experimentally study the properties of supercooled water at atmospheric pressure in the whole temperature range, from the melting point of water to the glass-transition temperature.

Since the development of mesoporous materials such as MCM-41 extensive studies of confined water have been carried out below the homogeneous nucleation temperature (T_H) [3,6–10]. Meanwhile, there are few studies on the temperature dependence of confined water in liquids. In this article, we use a reverse micellar solution for such studies. The water does not freeze below T_H in a reverse micellar solution, and the confinement of water due to its cage by a reverse micelle is significantly reduced at low temperatures. Further, the reduction of confinement is well explained in terms of water shedding from the reverse micelle.

A reverse micelle is a nanometer-scale cage filled with water [11–27]. The aqueous cavity radius of the reverse micelle is proportional to the water-surfactant molar ratio w_0 (=[water]/[surfactant]), and can be controlled experimentally [11,12]. Water in reverse micelles has been studied below the melting point of water by several experimental methods [20–24], and these studies have demonstrated that freezing temperatures obtained for the reverse micelles at large w_0 ($w_0 \gtrsim 5$) are above T_H, which implies that reverse micelles at large w_0 do not have a strong effect on lowering the water's freezing temperature. Therefore, in order to explore the possibility that the freezing temperature of confined water can be lowered by reverse micelles, it is necessary to examine reverse micelles at small w_0, i.e., $w_0 \lesssim 5$. However, contradictory results were reported for reverse micelles at small w_0 values. A neutron scattering study of AOT [= bis(2-ethyl-hexyl)sulfosuccinate, surfactant] reverse micelles on nanosecond time scales has demonstrated that the freezing temperature of confined water depends on w_0 in the w_0 range from 3 to 40 [20]. Here we note that such a measurement cannot rule out the existence of water dynamics on time scales longer than nanoseconds. On the contrary, a study using differential scanning calorimetry (DSC) for water/AOT/isooctane above ∼200 K has shown that no freezing of water occurs at $w_0 <$ 4.5 [21], although an interaction between reverse micelles could affect the freezing behavior under the experimental conditions of high volume fractions of the reverse micelle. In addition, the DSC measurements cannot indicate whether frozen water resides inside or outside the reverse micelles.

We use a water-soluble molecule, rhodamine 6G [24–26], as a probe for studying water in a reverse micellar solution and measure the optical absorption spectra of the molecule. The fluctuation and relaxation of the electronic energy of the probe molecule in solution occur due to the motion of the solvent molecules (water in the present study) which interact with the probe molecule. Extensive studies of various dye solutions [28–31], including a dye aqueous solution [32], have demonstrated that the relaxation processes, such as the diffusion one, in liquids and supercooled liquids can be studied by using a dye molecule as a probe and optical spectroscopy of the probe molecule. This means that the interaction between the dye molecule and the surrounding solvent molecules is so weak that the dye molecule almost does not alter the intrinsic dynamic behavior of the liquid's molecules, although the interaction could distort the structure of the liquid. Thus, in the present study, we have measured the temperature dependence of the absorption spectra due to the π-π^* electronic transition of rhodamine 6G in AOT/isooctane reverse micellar solutions at $w_0 = 2$, 3, and 5. The reverse micelles at $w_0 = 2$, 3, and 5 are estimated to have aqueous cavity radii of 0.81, 0.95, and 1.22 nm, 81, 148, and 338 water molecules, and 41, 49, and

*Corresponding author: murakami.hiroshi@jaea.go.jp

68 AOT molecules, respectively, where the dye molecule is assumed to be a sphere with a radius of 0.5 nm [18].

II. EXPERIMENT

The sample was prepared by the injection method [18]. The concentrations of rhodamine 6G and AOT were $\sim 1 \times 10^{-5} M$ and $0.1 M$, respectively. The volume fractions of reverse micelles were below 0.1. The dye molecule is not dissolved in isooctane. Further, it has been found from AOT concentration dependence of the absorption spectrum of the rhodamine 6G aqueous solution that the absorption spectrum of this molecule changes drastically owing to the interaction with the surfactant molecule. As for the dye molecule in the reverse micellar solution, no drastic changes in the spectral feature were observed in the temperature range examined. Hence, the solvation shell of the dye molecule is considered to consist of water molecules over the temperature range examined.

A double-beam absorption spectroscopy system with a spectral resolution of ~ 10 cm^{-1} was used. The temperature of the sample was controlled within ± 0.5 K by a nitrogen-continuous-flow cryostat, and the rate of decreasing temperature was below 0.5 K/min. The absorption spectra were measured every 5 K in the temperature range from room temperature to ~ 170 K, which is about the melting point of isooctane; however, for the sample at $w_0 = 5$ the lower limit was ~ 220 K. Gradual growth of the absorption spectrum's baseline on a 10-min time scale was observed at ~ 220 K and $w_0 = 5$ owing to Tyndall scattering, and finally the sample became opaque; however, the solution did not freeze. On the other hand, for $w_0 = 2$ and 3 the baseline does not change in the temperature range examined. These results are supported by the DSC measurement [21]. Thus, below we focus on the results for $w_0 = 2$ and 3.

III. RESULTS AND DISCUSSION

To analyze the absorption spectra of the sample we use the configuration coordinate (CC) model, because the spectra are well fitted by Gaussian curves (see the Appendix), as observed for rhodamine 6G in various solutions [30,33]. In the CC model [30,33–38], the potential curves of the electronic ground and excited states of a dye molecule in solution are given by $U_g(Q) = aQ^2$ and $U_e(Q) = a(Q - Q_0)^2 + E'$, respectively, as shown in Fig. 1(a). The configuration coordinate (Q) corresponds to the configuration of the solvent molecules that surround the dye molecule. In the liquid state, the thermal equilibrium is achieved by the configurational fluctuation due to diffusional motions of the solvent molecules. Therefore we can use the Boltzmann distribution for the population distribution in the electronic ground state, and the absorption spectrum of the dye molecule is given by

$$I(\omega) = A \exp\left[-\frac{(\omega - E)^2}{\sigma}\right], \tag{1}$$

with $E \equiv E' + aQ_0^2 + \Delta$ and $\sigma \equiv 4k_B T(aQ_0^2 + \Delta)$. Here k_B and T are the Boltzmann constant and absolute temperature, respectively. The quantity Δ is the lattice relaxation energy, and determines the spectral broadening due to the phononlike

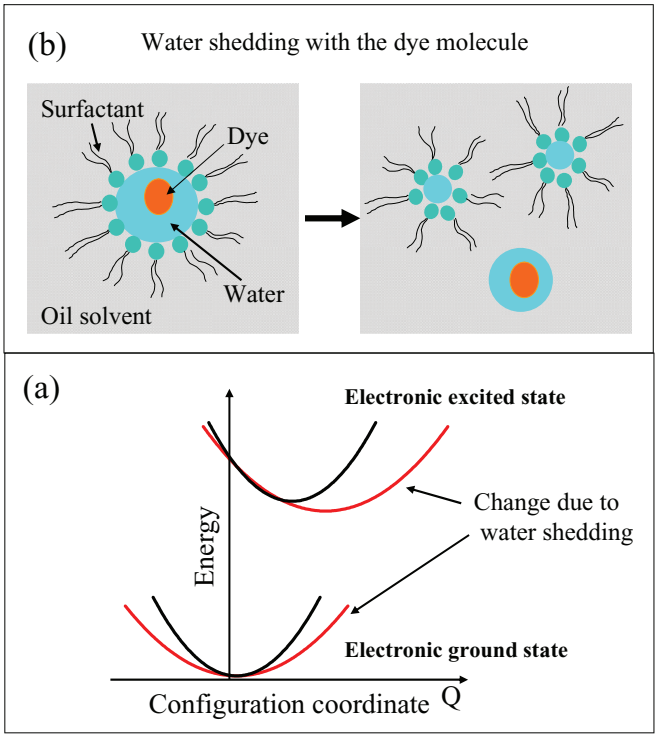

FIG. 1. (Color online) (a) Adiabatic potential curves of the electronic excited and ground states of a dye molecule in a reverse micellar solution as a function of a configuration coordinate. Change in the potential curves on water shedding from the reverse micelle is schematically shown by red curves. (b) Schematic cross-section diagrams of the dye-molecule-containing reverse micelle before (left) and after the water shedding with the dye molecule (right).

motions of the matrix (including the internal motions of the dye molecule) [30,36,38]. This relaxation is very fast (<1 ps), and so the thermal equilibrium is established for this relaxation mode independently of temperature. The parameter σ determines the spectral width and is proportional to the temperature with a proportionality constant of $4k_B(aQ_0^2 + \Delta)$ in the liquid state. On the other hand, below the glass-transition temperature T_g, σ is given by $4k_B(aQ_0^2 T_g + \Delta T)$ and varies with temperature with a proportionality constant of $4k_B\Delta$, because the configurational fluctuation of the surroundings of the dye molecule is frozen, that is, the temperature of the Boltzmann distribution for the coordinate Q is put at $T = T_g$. Hence, if σ is plotted versus temperature, the graph bends at T_g, as seen in Fig. 2, allowing for an estimation of the glass-transition temperature from the temperature dependence of σ [30,37–40]. Further, if the graph of σ is extrapolated to $T = 0$, the Y intercept is zero in the liquid state, whereas it is nonzero ($4aQ_0^2 k_B T_g$) in the glass state.

Temperature dependences of σ obtained by the Gaussian curve fitting using Eq. (1) of the absorption spectra are shown in Fig. 3. There are three temperature ranges which yield different slopes at $w_0 = 2$ and 3; we refer to these ranges as I, II, and III, in order of decreasing temperature. The results obtained by linear curve fitting for each temperature range are plotted as solid lines in Fig. 3. The values of the slope (α) and Y intercept (β) are given in the figure caption.

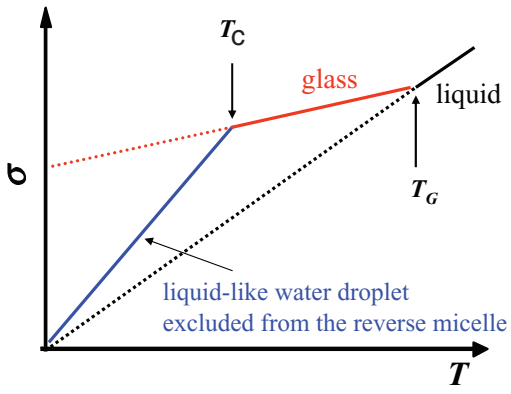

FIG. 2. (Color online) Schematic diagram of the temperature dependence of the spectral width parameter σ for the dye-molecule-containing water droplet. Below T_C, the droplet excluded from the reverse micelle is not constrained by the reverse micelle and its water molecules attain diffusionlike motion.

The values of the Y intercept are not zero, but fairly large at $w_0 = 2$ and 3 in temperature range I, and so the configurational fluctuation of the dye molecule's surroundings is considered to be frozen in range I. This happens because the configurational fluctuation is constrained owing to the tight space as well as to a small amount of water in the reverse micelle. Fluorescence measurements of dye molecules in AOT reverse micelles have suggested that the dye molecule's surroundings are frozen at room temperature at low w_0 values [26,27]. Further studies, however, will be necessary to determine whether the configurational fluctuation is frozen completely or partially; we note that there are glass-forming materials which the two-dimensional CC model needs to be applied to [38]. The slope of the graph at $w_0 = 2$ is about half of the value at $w_0 = 3$. This seems to reflect the effect of the number of water molecules, i.e., the reverse micelle size, on the density of states

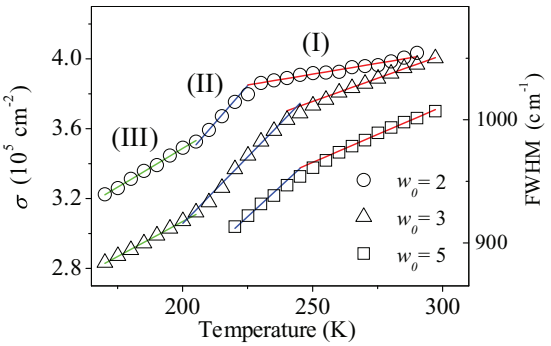

FIG. 3. (Color online) Temperature dependence of σ in the reverse micellar solution at $w_0 = 2$, 3, and 5, shown by symbols. Solid lines show the results due to linear curve fitting [$\alpha T + \beta$; α: slope (cm^{-2} K^{-1}); T: temperature; β: Y intercept (10^5 cm^{-2})] of the data. The parameter values obtained by the fitting are as follows. Temperature range I: $w_0 = 2$ ($\alpha = 290$, $\beta = 3.19$), $w_0 = 3$ ($\alpha = 540$, $\beta = 2.42$), $w_0 = 5$ ($\alpha = 640$, $\beta = 1.8$); range II: $w_0 = 2$ ($\alpha = 1710$, $\beta = 0$), $w_0 = 3$ ($\alpha = 1530$, $\beta = 0$), $w_0 = 5$ ($\alpha = 1380$, $\beta = 0$); range III: $w_0 = 2$ ($\alpha = 890$, $\beta = 1.71$), $w_0 = 3$ ($\alpha = 820$, $\beta = 1.44$). FWHM is the full width at half maximum, which is derived from $2\sqrt{\sigma \ln 2}$.

of vibrational modes, because the slope is given by $4k_B\Delta$ in the CC model, if the surroundings of the dye molecule are glasslike.

In temperature range II, the slopes of the graphs for $w_0 = 2$ and 3 increase remarkably compared with those in range I, and the graphs bend at ~225 K ($w_0 = 2$) and ~240 K ($w_0 = 3$). The graphs for $w_0 = 2$ and 3 can be fitted by linear curves with a Y intercept of 0 in range II, as seen in Fig. 3. According to the CC model, the configurational fluctuation of the dye molecule's surroundings is in the thermal equilibrium, that is, in the liquid state, in range II. This indicates that the confinement responsible for the freezing of the configurational fluctuation in temperature range I changes drastically, and is significantly reduced in range II. This leads to the fact that the potential curves of the dye molecule are altered in range II, as seen in Fig. 1(a). In addition to the change in the value of a, larger energy relaxation in the electronic excited state will occur in range II, because water molecules surrounding the dye molecule attain a larger configurational change owing to reduction in the constraint of the reverse micelle, and eventually the coordinate of Q_0 becomes larger. Therefore, the slope of the graph in range II can be steeper than that in the liquid state at higher temperatures, owing to a change in the value of aQ_0^2 responsible for the slope, as is schematically described in Fig. 2. This provides an explanation for the temperature dependence of σ in range II. The above

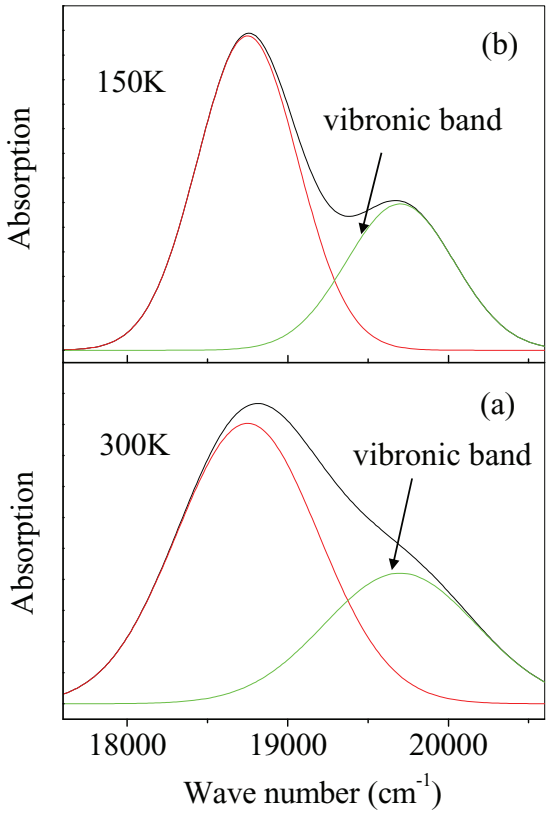

FIG. 4. (Color online) The spectra calculated from Eq. (A1) at (a) 300 K and (b) 150 K. The parameter values are as follows: $A_1 = 1$, $E_1 = 18\,750$ cm^{-1}, $\kappa_1 = 1300$ cm^{-2} K^{-1}, $A_2 = 0.5$, $E_2 = 19\,700$ cm^{-1}, $\kappa_2 = 1500$ cm^{-2} K^{-1}.

discussions for ranges I and II are also valid for the result at $w_0 = 5$.

In region III, the slopes of the graphs at $w_0 = 2$ and 3 decrease compared with those in region II, and the Y intercepts are nonzero. Hence, freezing of the configurational fluctuation of the dye molecule's surroundings is considered to occur at ~210 K. In addition to the singularity of thermodynamic behavior of supercooled water at ~228 K [1–3], it has been proposed that the fragile-to-strong liquid transition (FST) would occur in water at around 228 K [41]. Further, it has been demonstrated that such a transition occurs in water confined in mesoporous materials at ~224 K [7] and 215 K [8]; however, it should be noted that there are several studies that question the interpretation in terms of FST [9,42–44]. The transitionlike behavior observed at ~210 K in the present study may be related to these phenomena, although the temperature does not agree with the temperatures at which the phenomena occur. The disagreement may be attributed to the presence of the dye molecule in the water droplet, because the hydrogen-bond network of water could be altered by the molecule in it.

In the rest of this paper, we discuss how the confinement of water by the reverse micelle is significantly reduced in temperature range II. First, we note that microparticles larger than several tens of nanometers due to aggregation will not be formed, because the Tyndall scattering is not observed at $w_0 = 2$ and 3 in the temperature range examined (above ~220 K for $w_0 = 5$). Second, it has been found from the low-temperature measurements that water is observed at the bottom of the sample cell of the reverse micellar solution above $w_0 = 5$, that is, a biphasic water-oil system forms, after the temperature returns to room temperature from below; for the samples below $w_0 = 3$, the amount of water was too small to observe the phenomenon. This phenomenon was also reported for an AOT/pentane reverse micellar solution, and the dynamics of water shedding from the reverse micelle was demonstrated [22]. Hence, we consider that water shedding from the reverse micelle occurs at low temperatures in the samples examined, and the water droplet that is expelled is dispersed without the formation of microparticles. The water will become free from the confinement of the reverse micelle's cage upon water shedding, and so the constraint on water's motion in the droplet will be significantly weaker. Moreover, on the basis of the fact that water surrounding the dye molecule is liquidlike in range II, water, together with the dye molecule, will be expelled from the reverse micelle upon the water shedding [see Fig. 1(b)]. Thus, the reduction in the confinement in range II is well explained in terms of water shedding. On the other hand, it is considered that the reverse micelles that lose water are also dispersed after water shedding [Fig. 1(b)], because the reverse micelle at smaller

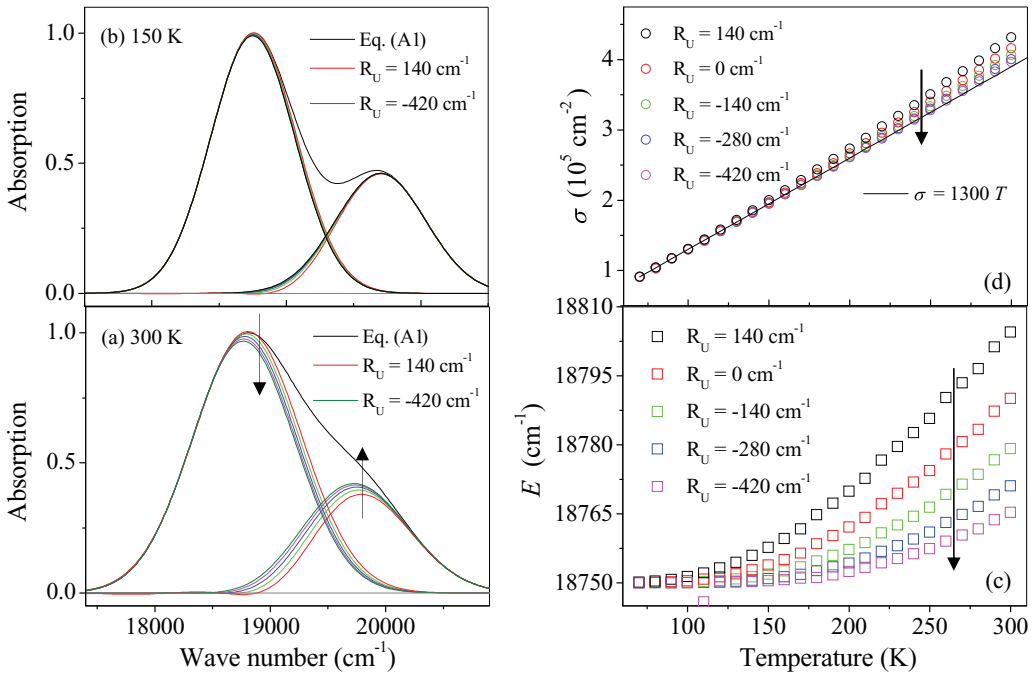

FIG. 5. (Color online) Results of the Gaussian curve fitting using Eq. (1) of the absorption spectrum calculated from Eq. (A1) at (a) 300 K and (b) 150 K on the low-frequency side of the spectrum. The residual curves are also depicted. The absorption maximum is normalized to unity. We note that the frequency at the absorption maximum changes with temperature. Therefore, the upper limit (R_U) of the data range for the fitting is defined by the frequency difference from the absorption maximum; positive values of R_U mean the position on the high-frequency side from the absorption maximum. The values of R_U are 140 cm^{-1} (red), 0 cm^{-1} (green), -140 cm^{-1} (blue), -280 cm^{-1} (purple red), and -420 cm^{-1} (olive). The lower limit of the data range for the fitting is set at the frequency that leads to 0.1 of the absorption amplitude on the low-frequency side; this value, however, has no effect on the result of the fitting, because the tail of the absorption spectrum in the low-frequency region is Gaussian without the effects of the vibronic band. (c) and (d) Temperature dependences of E and σ obtained by the fitting. The temperature dependence of σ at $\kappa_1 = 1300$ cm^{-2} K^{-1} is shown by a solid line in (d). The value of R_U decreases according to the direction of the arrows.

w_0 values is preserved at lower temperatures. However, the present experimental study does not rule out the formation of some nanometer-scale structure which is different from the surfactant-free water droplet including the dye molecule and leads to a weaker confinement for the water and dye molecules in range II.

The suggestion [23] that the shrinking of reverse micelles observed by a neutron scattering study is caused by water shedding is supported by the following findings. First, the temperatures (T_C) at which the graphs for $w_0 = 3$ and 5 in Fig. 3 bend between ranges I and II roughly correspond to the temperature (T_S) at which the shrinking occurs at the same w_0. Second, the dependence of T_S on w_0 shows the same trend as that of T_C. Finally, the shrinking of the reverse micelle cannot be explained in terms of the division of one reverse micelle into some smaller reverse micelles because of the lack of surfactant molecules for the small reverse micelles [13]. On the other hand, the shrinking of AOT reverse micelles and w_0 dependence of T_S are observed in several oil solvents [22,23]. This suggests that shrinking of the reverse micelle occurs owing to water shedding in an AOT reverse micelle irrespective of the solvent type.

IV. CONCLUSION

Confined water in mesoporous materials is widely used for the investigation of supercooled water, but there has been an issue regarding the interaction between confined water and the internal surface of the cage used for the confinement [3]. The surroundings of confined water that is used for studies of supercooled water should only weakly affect its properties. Thus, we consider that water in a reverse micellar solution is a promising candidate for studying supercooled water, for the following reasons: (1) The confinement of water due to the cage of the reverse micelle is significantly reduced, (2) the water is in the supercooled state below T_H, (3) it exhibits a transitionlike behavior below T_H, and (4) it is confined in liquid. Furthermore, there are a variety of reverse micelles, and different types of reverse micelles are also being produced. A water droplet in a reverse micellar solution at low temperatures will show different features regarding the confinement, depending on the types of surfactants and solvents used. Hence, it will be possible to examine a variety of water droplets with these different confinements, and the sizes and surroundings of the water droplet could be chemically controlled at low temperatures. Thus, further studies of the reverse micellar solution by various experimental methods, including structural characterization of samples, in a wide temperature range, the lower limit of which is determined by the melting point of oil solvents, will provide information complementary to the results previously obtained for supercooled water.

ACKNOWLEDGMENTS

The authors thank Dr. K. Akamatsu, Dr. N. Shikazono, and Dr. A. Tanaka for fruitful discussions. This study was partly supported by Grants-in-Aid for Scientific Research (23654139).

APPENDIX: GAUSSIAN CURVE FITTING OF THE ABSORPTION SPECTRUM

The absorption spectra of dye molecules in various solutions exhibit a Gaussian spectral shape in the low-frequency region from the absorption maximum, and a discrepancy between the spectra and Gaussian curve is seen on the high-frequency side because of the existence of the vibronic levels of the dye molecule and the asymmetric-Gaussian character of the electronic absorption band [30,33–35,37,38]. In this

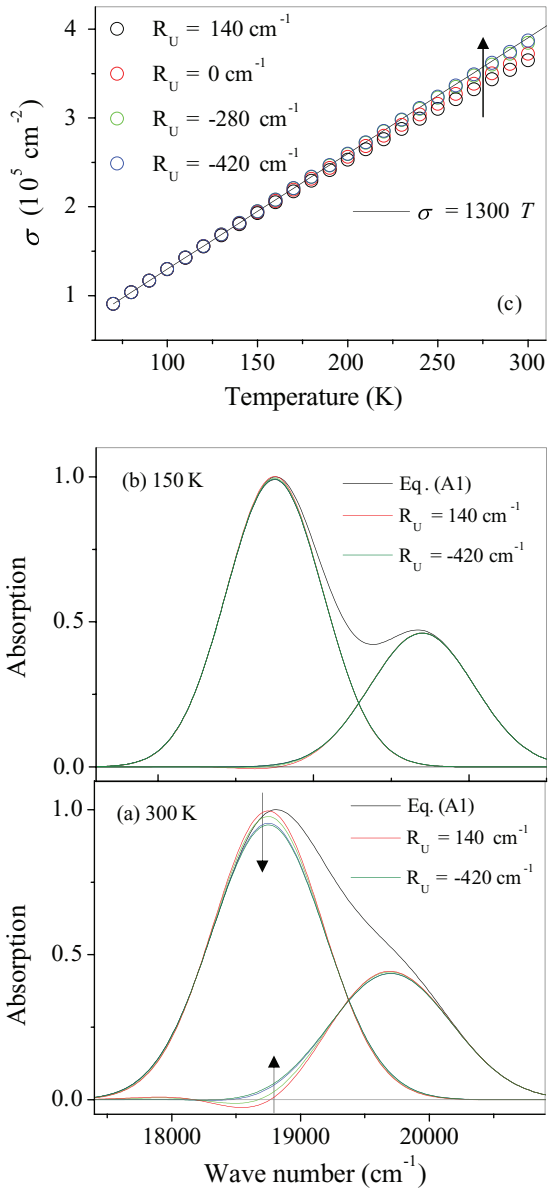

FIG. 6. (Color online) Results of the Gaussian curve fitting using Eq. (1) with $E = 18\,750\ \mathrm{cm}^{-1}$ of the absorption spectrum calculated from Eq. (A1) at (a) 300 K and (b) 150 K on the low-frequency side. The residual curves are also depicted. The absorption maximum is normalized to unity. The values of R_U are 140 cm^{-1} (red), 0 cm^{-1} (green), $-280\ \mathrm{cm}^{-1}$ (blue), and $-420\ \mathrm{cm}^{-1}$ (olive). The lower limit is set at the frequency that leads to 0.1 of the absorption amplitude in the low-frequency region. (c) Temperature dependence of σ obtained by the fitting. The value of R_U decreases according to the direction of the arrows.

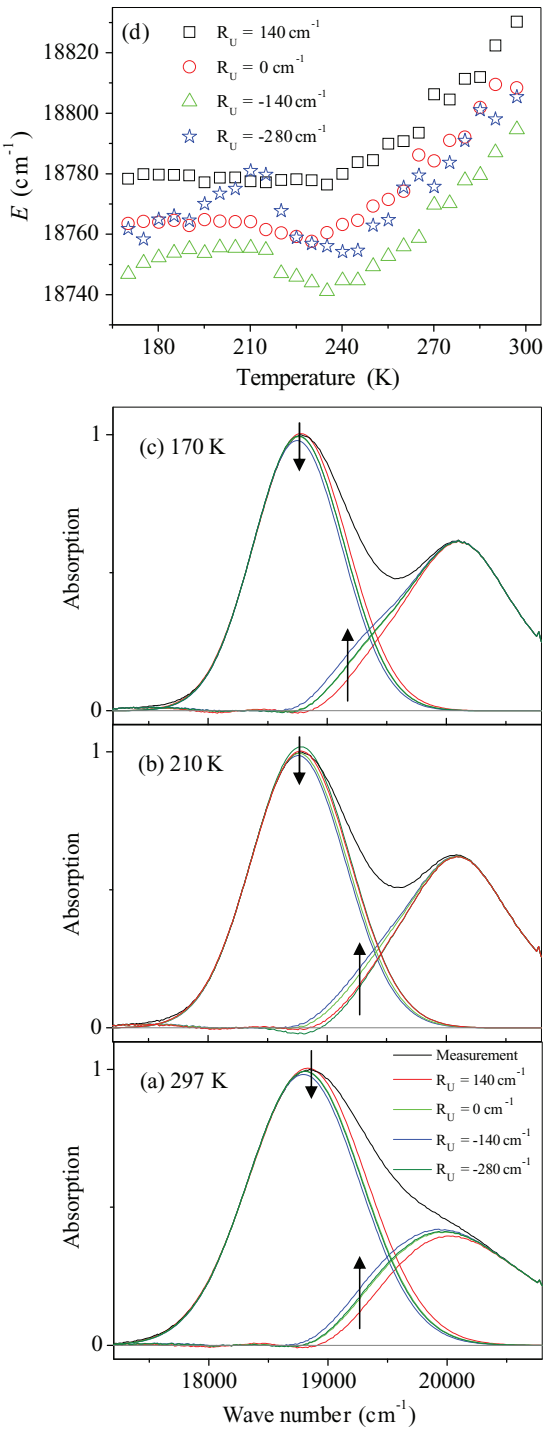

FIG. 7. (Color online) Results of the Gaussian curve fitting using Eq. (1) of the absorption spectra measured at (a) 297 K, (b) 210 K, and (c) 170 K. The residual curves are also depicted. The absorption maximum is normalized to unity. (d) Temperature dependence of E obtained by the fitting. The value of R_U decreases according to the direction of the arrows except for $R_U = -280$ cm^{-1}. The Gaussian curves at $R_U = -280$ cm^{-1} almost coincide with those at $R_U = 0$ cm^{-1} in (a) and (c), whereas it has the largest amplitude in (b).

Appendix, we describe the procedure of Gaussian curve fitting of the absorption spectrum in the low-frequency range to obtain the value of σ in Eq. (1).

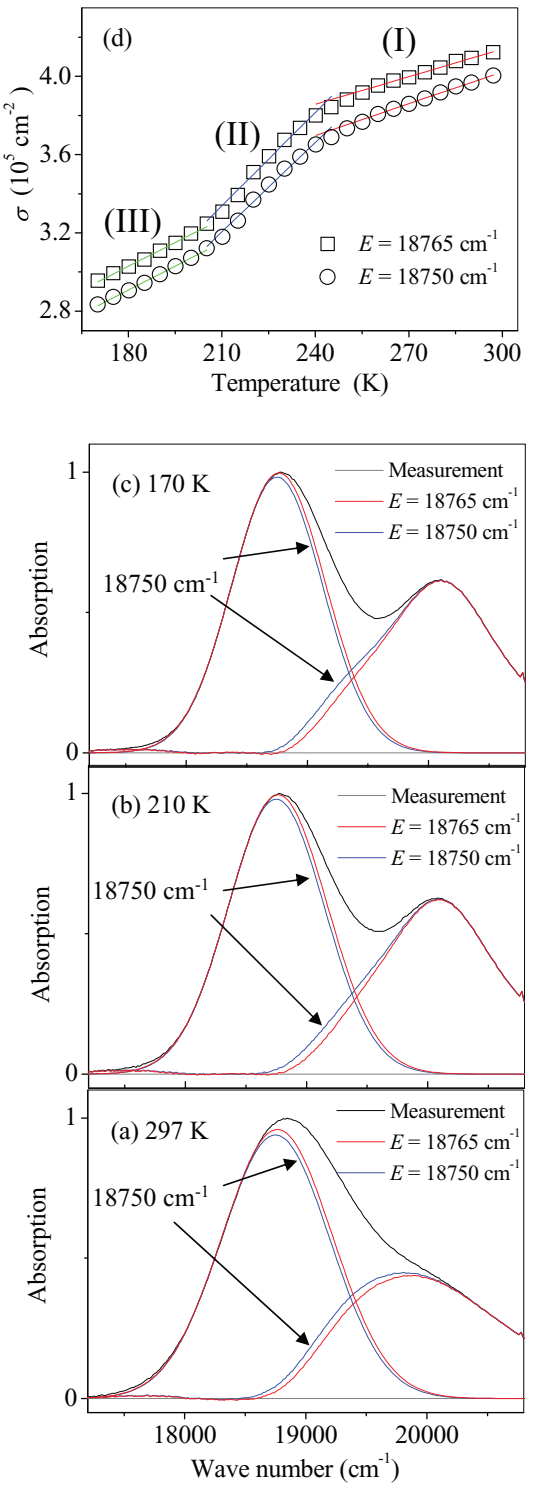

FIG. 8. (Color online) Results of the Gaussian curve fitting using Eq. (1) with $E = 18\,750$ and $18\,765$ cm^{-1} of the absorption spectra measured at (a) 297 K, (b) 210 K, and (c) 170 K. The residual curves are also depicted. The absorption maximum is normalized to unity. (d) The temperature dependence of σ obtained by the fitting. The parameter values for solid lines [$\alpha T + \beta$; α: slope (cm^{-2}K^{-1}); T: temperature, β: Y intercept (10^5 cm^{-2})] are as follows. Temperature range I (red): $E = 18\,750$ cm^{-1} ($\alpha = 540$, $\beta = 2.4$), $E = 18765$ cm^{-1} ($\alpha = 470$, $\beta = 2.73$); range II (blue): $E = 18\,750$ cm^{-1} ($\alpha = 1530$, $\beta = 0$), $E = 18\,765$ cm^{-1} ($\alpha = 1590$, $\beta = 0$); range III (green): $E = 18\,750$ cm^{-1} ($\alpha = 820$, $\beta = 1.44$), $E = 18\,765$ cm^{-1} ($\alpha = 810$, $\beta = 1.58$).

First, we demonstrate the effect of the vibronic band on the fitting by use of a model absorption spectrum given by a sum of two Gaussian functions, i.e.,

$$I_0(\omega) = A_1(\sigma_1\pi)^{-\frac{1}{2}} \exp\left[-\frac{(\omega - E_1)^2}{\sigma_1}\right] + A_2(\sigma_2\pi)^{-\frac{1}{2}} \times \exp\left[-\frac{(\omega - E_2)^2}{\sigma_2}\right] (\sigma_1 = \kappa_1 T,\ \ \sigma_2 = \kappa_2 T). \tag{A1}$$

The first term is due to the electronic absorption band, and the second one is to the vibronic band; we note that one vibronic level is assumed to contribute to the spectrum, although many levels will actually contribute to it. Here, parameter $\sigma_i (i = 1,2)$ is proportional to the temperature with a proportionality constant of κ_i. Figure 4 shows the spectra (black) calculated from Eq. (A1) at 300 and 150 K, together with the two components [red (dark gray): electronic band; green (light gray): vibronic band]. It is found that agreement between the absorption spectrum (black) and the electronic band (red) around the absorption maximum is not good at 300 K, compared with at 150 K, owing to the presence of the broader vibronic band at 300 K.

Figure 5 shows results of the Gaussian curve fitting using Eq. (1) of the absorption spectrum calculated from Eq. (A1) in several data ranges on the low-frequency side of the spectrum, where we use a nonlinear least squares method of OriginPro for the fitting and set all the parameters in Eq. (1) as free parameters. The Gaussian curve obtained by the fitting depends on the upper limit (R_U) of the data range of the fitting (see the figure caption for the definition of R_U) considerably at 300 K, and the level of agreement in the curve fitting is low at $R_U = 140$ and $0\ \mathrm{cm}^{-1}$ because the residual curve has a negative region. The values of E obtained by the fitting converge to $18\,750\ \mathrm{cm}^{-1}$, at which E_1 is put in calculating the absorption spectrum, in Fig. 5(c) irrespective of R_U at low temperatures. On the other hand, as seen in Fig. 5(d), the temperature-dependent variation of σ for all R_U values deviates from that of $\sigma = 1300T$ for the electronic absorption band calculated above ~150 K. Thus, the temperature dependence of σ is not properly derived by the fitting owing to the presence of the vibronic band if all the parameters in Eq. (1) are free, whereas we can obtain the proper value of E as a definite value at low temperatures.

The results of the Gaussian curve fitting using Eq. (1), where the value of E is fixed at $18\,750\ \mathrm{cm}^{-1}$, are shown in Fig. 6. The Gaussian curve obtained by the fitting depends on R_U considerably at 300 K, and the level of agreement in the curve fitting is low at $R_U = 140$ and $0\ \mathrm{cm}^{-1}$ because the residual curve has a negative region. Further, the temperature dependence of σ at $R_U = -280$ and $-420\ \mathrm{cm}^{-1}$ coincides with that of $\sigma = 1300T$ in Fig. 6(c), but it does not at $R_U = 140$ and $0\ \mathrm{cm}^{-1}$. Thus, it is considered that the value of σ for the electronic absorption band can be properly obtained by the Gaussian curve fitting of the absorption spectrum which has a vibronic band on the high-frequency side, if E is fixed at the proper value and if the Gaussian curve fitting goes well in proper data ranges for the fitting.

On the basis of the above results, we first perform the Gaussian curve fitting of the measured absorption spectrum in several data ranges and with all the parameters in Eq. (1) as free parameters to obtain a proper value of E. If the value of E is determined, the Gaussian curve fitting, with a fixed value of E, is next done in several data ranges. We present the results obtained for $w_0 = 3$. The absorption spectra measured at 297, 210, and 170 K, together with the Gaussian curves obtained by the fitting and the residual curves, are depicted in Figs. 7(a)–7(c), respectively. The temperature dependence of E obtained by the fitting is plotted in Fig. 7(d), and it is found that E converges to a definite value at low temperatures, except for the case at $R_U = -280\ \mathrm{cm}^{-1}$, and that the definite value depends on R_U. The curve fitting does not go well at $R_U = -280\ \mathrm{cm}^{-1}$, as obviously seen in Fig. 7(b), and so this R_U value is not considered to be appropriate for the fitting. Agreement between the measured spectrum and the curve obtained by the fitting at $R_U = 140\ \mathrm{cm}^{-1}$ is also not very good around the absorption maximum in the temperature range examined. According to the convergence of the E value at low temperatures and the level of agreement in the curve fitting, the Gaussian curve fitting is performed at $E = 18\,750$ and $18\,765\ \mathrm{cm}^{-1}$, and the results are shown in Fig. 8. The temperature dependences of σ obtained by the fitting at the two values of E show the same behavior, that is, three temperature ranges with different slopes, although the Gaussian curves obtained by the fitting are different at the same temperature. Further, the values of the slopes and Y intercepts in the same temperature range are roughly the same between the results at the two E values (see the figure caption for the values). Hence the conclusion drawn in the main text does not depend on the E values used. The temperature dependence of σ obtained at $E = 18750\ \mathrm{cm}^{-1}$ is used for Fig. 3. The temperature dependences of σ for $w_0 = 2$ and 5 are obtained in the same way.

[1] C. A. Angell, Annu. Rev. Phys. Chem. **34**, 593 (1983); in *Water: A Comprehensive Treatise*, edited by F. Franks (Plenum, New York, 1982), Vol. 7, p. 1.

[2] O. Mishima and H. E. Stanley, Nature (London) **396**, 329 (1998).

[3] H. E. Stanley, S. V. Buldyrev, P. Kumar, F. Mallamace, M. G. Mazza, K. Stokely, L. Xu, and G. Franzese, J. Non-Cryst. Solids **357**, 629 (2011).

[4] N. Giovambattista, C. A. Angell, F. Sciortino, and H. E. Stanley, Phys. Rev. Lett. **93**, 047801 (2004).

[5] S. Capaccioli and K. L. Ngai, J. Chem. Phys. **135**, 104504 (2011).

[6] J. S. Beck, J. C. Vartuli, W. J. Roth, M. E. Leonowicz, C. T. Kresge, K. D. Schmitt, C. T.-W. Chu, D. H. Olson, E. W. Sheppard, S. B. McCullen, J. B. Higgins, and J. L. Schlenker, J. Am. Chem. Soc. **114**, 10834 (1992).

[7] L. Liu, S.-H. Chen, A. Faraone, C.-W. Yen, and C.-Y. Mou, Phys. Rev. Lett. **95**, 117802 (2005).

[8] P. Gallo, M. Rovere, and S.-H. Chen, J. Phys. Chem. Lett. **1**, 729 (2010).

[9] J. Hedström, J. Swenson, R. Bergman, H. Jansson, and S. Kittaka, Eur. Phys. J. Spec. Top. **141**, 53 (2007).
[10] K. Yoshida, T. Yamaguchi, S. Kittaka, M-C. Bellissent-Funel, and P. Fouquet, J. Phys.: Condens. Matter **24**, 064101 (2012).
[11] *Structure and Reactivity in Reverse Micelles*, edited by M. P. Pileni (Elsevier, Amsterdam, 1989).
[12] *Reverse Micelles*, edited by P. L. Luisi and B. E. Straub (Plenum, New York, 1984).
[13] A. Amararene, M. Gindre, J.-Y. Le Huérou, W. Urbach, D. Valdez, and M. Waks, Phys. Rev. E **61**, 682 (2000).
[14] G. Onori and A. Santucci, J. Phys. Chem. **97**, 5430 (1993).
[15] J. E. Boyd, A. Briskman, V. L. Colvin, and D. M. Mittleman, Phys. Rev. Lett. **87**, 147401 (2001).
[16] D. E. Moilanen, E. E. Fenn, D. Wong, and M. D. Fayer, J. Phys. Chem. B **113**, 8560 (2009).
[17] D. Cringus, A. Bakulin, J. Lindner, P. Vöhringer, M. S. Pshenichnikov, and D. A. Wiersma, J. Phys. Chem. B **111**, 14193 (2007).
[18] H. Murakami, T. Nishi, and Y. Toyota, J. Phys. Chem. B **115**, 5877 (2011); H. Murakami, Y. Toyota, T. Nishi, and S. Nashima, Chem. Phys. Lett. **519-520**, 105 (2012).
[19] R. E. Riter, D. M. Willard, and N. E. Levinger, J. Phys. Chem. B **102**, 2705 (1998).
[20] T. Spehr, B. Frick, I. Grillo, and B. Stühn, J. Phys.: Condens. Matter **20**, 104204 (2008).
[21] C. Boned, J. Peyrelasse, and M. Moha-Ouchane, J. Phys. Chem. **90**, 634 (1986).
[22] A. K. Simorellis, W. D. V. Horn, and P. F. Flynn, J. Am. Chem. Soc. **128**, 5082 (2006).
[23] T. Spehr, B. Frick, I. Grillo, P. Falus, M. Müller, and B. Stühn, Phys. Rev. E **79**, 031404 (2009).
[24] C. A. Munson, G. A. Baker, S. N. Baker, and F. V. Bright, Langmuir **20**, 1551 (2004).
[25] M. P. Heitz and F. V. Bright, Appl. Spectrosc. **49**, 20 (1995).
[26] M. Hasegawa, T. Sugimura, Y. Shindo, and A. Kitahara, Colloids Surf., A **109**, 305 (1996).
[27] G. B. Dutt, J. Phys. Chem. B **112**, 7220 (2008).
[28] R. Richert, Phys. Rev. B **54**, 15762 (1996).
[29] J. Ma, D. Vanden Bout, and M. Berg, Phys. Rev. E **54**, 2786 (1996).
[30] S. Kinoshita and N. Nishi, J. Chem. Phys. **89**, 6612 (1988).
[31] H. Murakami, Chem. Phys. Lett. **417**, 550 (2006).
[32] M. Maroncelli and G. Fleming, J. Chem. Phys. **89**, 5044 (1988).
[33] S. Kinoshita, N. Nishi, A. Saitoh, and T. Kushida, J. Phys. Soc. Jpn. **56**, 4162 (1987).
[34] H. Murakami and T. Kushida, Phys. Rev. B **54**, 978 (1996).
[35] J. S. Ahn, Y. Kanematsu, and T. Kushida, Phys. Rev. B **48**, 9058 (1993).
[36] Y. Toyozawa, *Optical Processes in Solids* (Cambridge University Press, Cambridge, UK, 2003).
[37] T. Kushida, J. S. Ahn, K. Hirata, and A. Kurita, Biochem. Biophys. Res. Commun. **160**, 948 (1989).
[38] H. Murakami, T. Kushida, and H. Tashiro, J. Chem. Phys. **108**, 10309 (1998).
[39] A. D. Pace, A. Cupane, M. Leone, E. Vitrano, and L. Cordone, Biophys. J. **63**, 475 (1992).
[40] V. Šrajer and P. M. Champion, Biochemistry **30**, 7390 (1991).
[41] K. Ito, C. T. Moynihan, and C. A. Angell, Nature (London) **398**, 492 (1999).
[42] W. Doster, S. Busch, A. M. Gaspar, M.-S. Appavou, J. Wuttke, and H. Scheer, Phys. Rev. Lett. **104**, 098101 (2010).
[43] S. Pawlus, S. Khodadadi, and A. P. Sokolov, Phys. Rev. Lett. **100**, 108103 (2008).
[44] S. Cerveny, J. Colmenero, and A. Alegría, Phys. Rev. Lett. **97**, 189802 (2006).